2 Challenges in Particle and Astroparticle Physics

Bernhard Spaan Wolfgang Rhode

Abstract: The elementary particles, the history, and the structure of our universe are studied in the physical disciplines of particle physics and astroparticle physics. Intending to study these fundamental processes and structures because of the expansion of the universe, both disciplines are closely connected. For this purpose, one can either study the high-energy interactions of particles in hot environments or analyze the information transmitted by messenger particles from distant events and sources in the universe. The former is studied in experiments at the Large Hadron Collider at CERN, the latter in various types of astroparticle detectors or telescopes. Both physical disciplines complement each other in the information accessible to them, are similar in the extreme demands placed on the resources required for data analysis and data quality, but differ due to the design and operation of the detectors in the generic properties of the collected data. Since the operation of the detectors is designed to answer specific fundamental questions, the guiding questions of particle and astroparticle physics are presented and explained in this chapter. Since many (if not all) of the later discussed exemplary applications of the computer science findings of the CRC 876 have been developed for the detectors LHCb, IceCube, MAGIC, FACT, and CTA, a special emphasis will be put on questions investigable with these detectors.

2.1 Physical Motivation, Problems, and Examples

In general, the epistemological considerations sketched in Chapter 1 do not only apply to the treatment of questions from a specific field of research; they claim general validity. However, this book is aimed at readers with different scientific backgrounds, so it seems appropriate to present a paradigmatic motivation for particle and astroparticle physics to which the examples given later may refer.

Our understanding of the physical world is essentially shaped by the two very successful theoretical standard models of cosmology and particle physics. The former focuses on the evolution of the universe in space and time, the latter on the interaction of its smallest particles. Both models are connected in many ways so that their statements complement but also control each other. Basically, both models are or were initially adapted to the cognitive preferences of man, symmetrical in theory—so symmetrical that for some time now, the justification of the asymmetry observed in the world has become a central research focus in the field of astrophysics and particle physics.

There are many fundamental questions that can be solved only by adding asymmetries to the standard models. Why do elementary particles have mass? Why is there more matter than antimatter? Why have no magnetic monopoles been detected (so far)? Why did the universe expand at different velocity scales? Why is matter distributed so differently in the universe? Why does dark matter exist? How (and where) can cosmic ravs gain energy?

The physical disciplines of particle physics and astroparticle physics try to find ways to clarify these questions in different types of experiments. In particle physics, high-energy elementary particles are shot at each other in terrestrial accelerators under very controlled conditions so that the symmetry of interactions can be studied under the energetic conditions of the early universe. In astroparticle physics, astronomical objects are used to accelerate particles to the highest energies. And either these messenger particles themselves or their interaction products are detected and interpreted on Earth. The challenges in astroparticle physics and particle physics are complementary. In particle physics, the conditions under which the first interaction occurs in the experiment are very well controlled. The experiments consist of different functioning inhomogeneous subdetectors in which data with different physical interpretations are recorded. In astroparticle physics, the detectors and, thus, the recorded data are comparatively homogeneous. However, the experimental conditions, such as the particle type, the location of the interaction, and its energy, cannot be controlled. Moreover, the detectors can change their properties with, e.g., the weather conditions, the incidence path through the surrounding natural media, or the time during the measurement.

2.2 Astroparticle Physics

Astroparticle physics is an approximately three-decade-old field of research [157] that has emerged from the extension of astronomy by experimental methods and theoretical concepts from particle physics. Its understanding is impossible without the current theoretical standard models of particle physics and cosmology and their possible extensions. Thus, it is based on the classical field theories (for gravity) and quantum field theories (for particle interactions), which have not yet been unified. The essential components of astroparticle physics are shown in Figure 2.1.

In astrophysical sources (such as stars, supernova remnants, the nuclei of active galaxies, and many other objects), temperatures are so high that matter must be considered as plasma (atomic nuclei and electrons are separated and move independently). The charged particles cause irregular magnetic fields and are vice versa, accelerated by these magnetic fields towards very high energies. The electrons and nuclei from the plasma can interact with other particles or emit radiation so that the sources can finally be observed from the detection of the light of electromagnetic radiation between the radio and gamma frequency ranges. Also, the neutrinos produced in hadronic interactions in the sources can be detected. A general glow in the sky of astroparticle

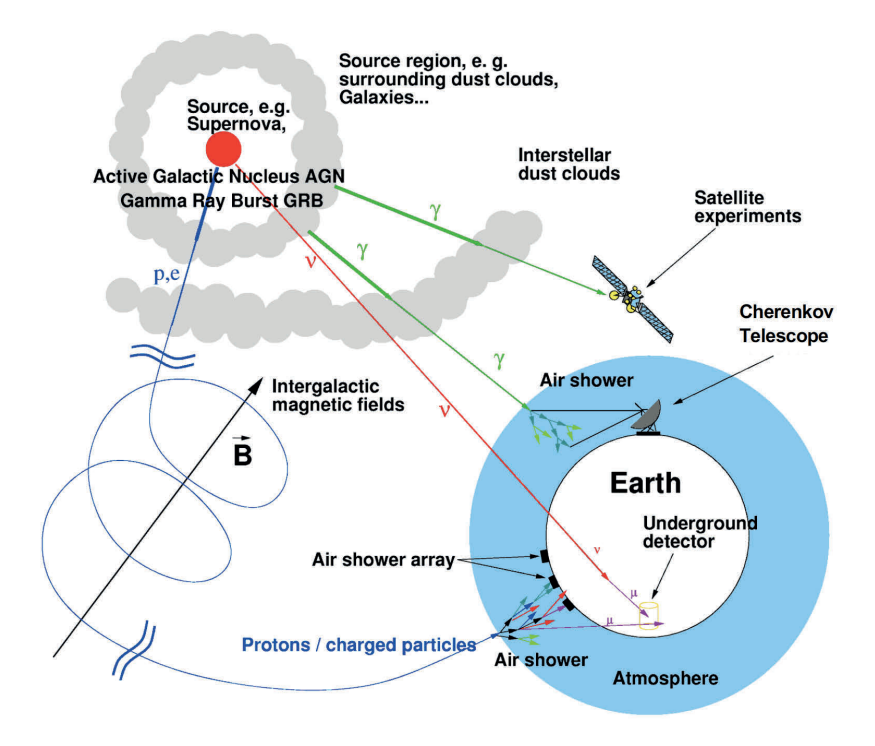


Fig. 2.1: Sketch of astroparticle physics. The figure shows the astronomical sources, the messenger particles, and the different detection scenarios (adapted from [385]).

physics is produced by the charged nuclei, which mostly lose their directional information when flying through the different magnetic fields on their way and are therefore of limited use for astronomical purposes. After repeated interactions, the follow-up products of astrophysical accelerations can be detected with different techniques using satellites, earthbound telescopes of different designs, and underground detectors. These individual and globally distributed detectors also use techniques developed in particle physics. To arrive at a complete understanding of astrophysical sources, the information from all detectors must be combined. At the latest, after this combination, the different components of the cosmic rays must be separated and understood.1

Depending on which of the three components contributing to the measurements (source properties, radiation propagation between the source and Earth, or interactions of elementary particles) is considered unknown, insights can be gained in astroparticle astrophysics, cosmology, or particle physics. Because of the complexity of the required physical descriptions and though much is known with precision, the assumption of

¹ For further discussion see [156].

completely controllable initial conditions cannot be made in this field. What is detected is the result of a concatenation of processes described by different theories and phenomenological approximations. In the end, these results may be precision measurements used, say, to close measurement gaps between experiments, test predicted signatures, or discover unexpected new phenomena that can only be explained by an extension of physical concepts. In the three decades of its existence, astroparticle physics has contributed to the revision of outdated theoretical ideas through many observations, despite or because of its complexity. And thus it might be well suited for the current discussion of epistemological boundary conditions of current physics using the science of big data.

In the historical development of physics one repeatedly finds dependencies between new physical insights and the new mathematical methods applied to them. The method of machine learning was developed in parallel to astroparticle physics. And it took some time until the early insight of computer science into the necessarily probabilistic nature of analytical results [280] was accepted in physics.

2.2.1 Experiments

From the field of astroparticle physics, two classes of experiments have given rise to and exemplified the development of machine learning methods in our work: neutrino telescopes and gamma telescopes, named after the messenger particle used to transmit information from the astrophysical source to Earth. Thus, both telescope types do not detect the astrophysical sources in the sky directly. They do not see the primary messenger particle but the Cherenkov light emitted from charged, high-energy secondary particles traversing a clear medium (water, ice). These secondary particles are produced in the form of an electromagnetic cascade in the atmosphere for primary gammas. In a charged current interaction of primary neutrinos, charged leptons (electrons, muon, taus) are produced. Also, a dominant part of the undesired background stems from the same source for both types of telescopes: cosmic rays in the form of atomic nuclei interact in the high atmosphere, also producing electromagnetic and hadronic cascades, including neutrinos. The background consists of the Cherenkov light induced by these particles and—depending on details of the data-taking—is many orders of magnitude stronger than the signal.

2.2.1.1 Neutrino Astronomy

Tim Ruhe

As stated above, neutrinos cannot be directly detected, and their detection thus relies on the detection of their leptonic partners, which are created in interactions with nuclei. Depending on the neutrino flavor, the interactions may happen either inside the detector or in the surrounding medium. The detection of neutrinos is nonetheless challenging due to their small interaction probability. This small interaction probability can, however, be accounted for by long exposure times, by utilizing large detection volumes or, ideally, by an optimized combination of both. As the detection of charged particles with velocities of approximately c (the speed of light in a vacuum) relies on the Cherenkov effect, and thus on the detection of Cherenkov photons, possible detection media also need to be as transparent as possible for blue light.

This requirement for transparent detection media with volumes of cubic kilometerscale leads to basically two natural media that can be utilized for the construction of neutrino telescopes: water and ice. Both options have been realized in practice and come with their very own experimental challenges. While water has been used for the neutrino telescopes Baikal [72], Antares [39] and KM3NetT [37], ice was used for AMANDA and IceCube [21].

When utilizing ice, one of the main challenges is the remote location of the telescopes, which requires sophisticated logistics during construction and operation. Fortunately, the South Pole is a location that offers large volumes of ice as well as research infrastructure via the Amundsen Scott South Pole station. Additional experimental challenges arise from the fact that water bubbles frozen in the ice cause a significant amount of light scattering. The amount of air bubbles, however, decreases with depth, and this challenge can be mitigated—at least to a certain extent—by deploying sensors at depths below 1500 m. Sensor deployment is carried out via the use of a hot water drill, and the deployment of sensors in a single borehole takes approximately 48 hours. After deployment, the sensors are frozen into place and cannot be accessed for maintenance. This thus requires the use of extremely reliable sensors, both in a mechanical and an electronic sense. The sensors used in IceCube were found to operate in an extremely reliable fashion, and in fact, most sensor failures did occur during deployment.

With respect to deployment and maintenance, the use of water is somewhat less challenging, as sensors and sensor units can be deployed by ship and also recovered for maintenance if necessary. Research infrastructures required for the operation of the telescopes are generally located at the coast in the vicinity of the installed telescopes. Although the scattering of Cherenkov photons only plays a minor role in water, two other main experimental challenges arise. The first one is associated with the decay of ⁴⁰K, which, due to its natural abundance, gives rise to increased noise rates observed by the sensors. A second challenge arises from the presence of bioluminescence in

the ocean, which also contributes to the increasing background noise recorded by individual sensors.

Although neutrino telescopes in ice and water are equally important for neutrino astronomy as they complement each other with respect to the utilized techniques but also with respect to the observation of certain parts of the sky. The remainder of this section will briefly introduce the IceCube detector. This is due to the fact that all neutrino-related analyses in this book use data obtained with the IceCube neutrino telescope. A brief understanding of the detector itself is thus a prerequisite for a comprehension of the analyses.

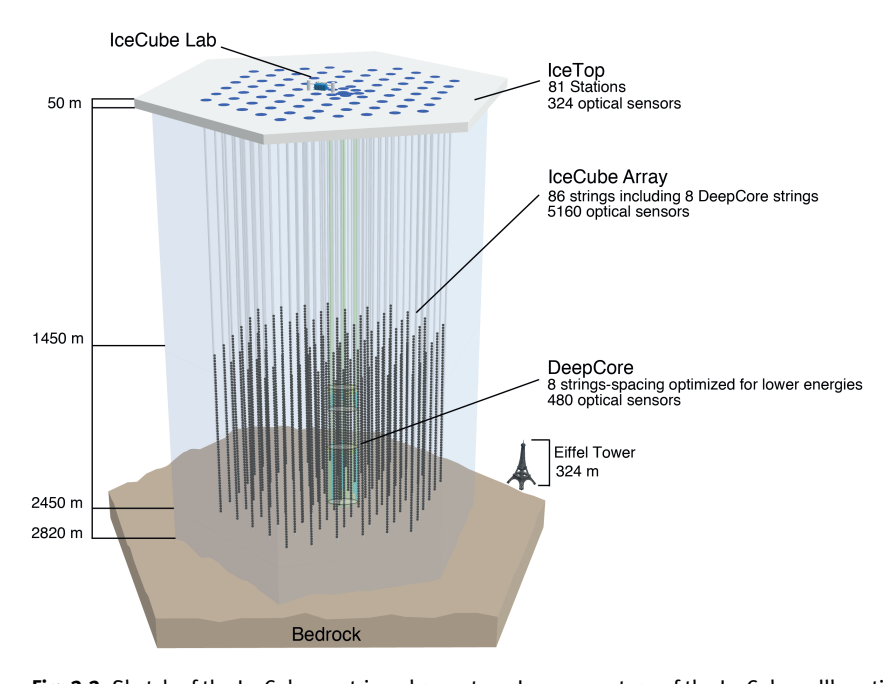


Fig. 2.2: Sketch of the IceCube neutrino observatory. Image courtesy of the IceCube collboration.

Figure 2.2 shows a schematic sketch of the IceCube neutrino observatory, located at the geographic South Pole. The detector consists of 86 strings arranged on a triangular grid with a string-to-string spacing of approximately 125 m. Strings in the center of the detector have a smaller spacing of roughly 70 m and form the DeepCore sub-detector. While the energy threshold of the entire in-ice array is $E_{\nu} \approx 100 \, \text{GeV}$, DeepCore is optimized for neutrino energies as low as $E_{\nu} \approx 10 \, \text{GeV}$.

IceCube strings are equipped with Digital Optical Modules (DOMs), which house a downward-facing 10" photomultiplier tube, as well as high voltage supply and readout electronics. The DOM-to-DOM distance on a string is 17 m, except for DeepCore strings, where the DOM spacing is only 7 m. In order to utilize the clear deep ice at the South

Pole, DOMs are deployed at a depth between 1450 m and 2450 m below the surface. The surface component IceTop, which serves as an air-shower array, completes the detector [21]. Although primarily designed for the detection of high-energy neutrinos from astrophysical sources, IceCube is a multi-purpose detector with a large scientific portfolio, as depicted in Figure 2.3.

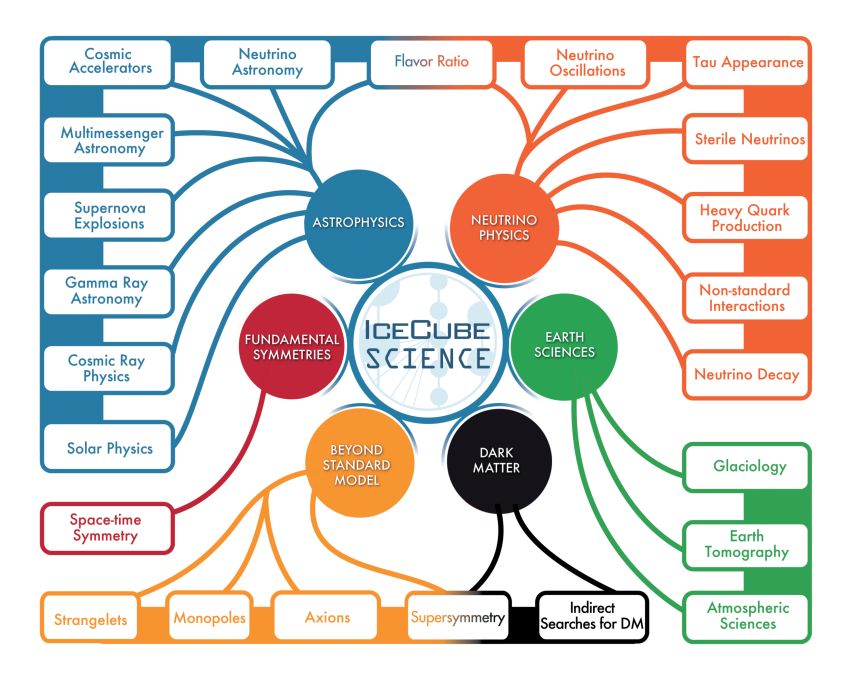


Fig. 2.3: The IceCube science portfolio. Graphic courtesy of the IceCube collaboration.

Although the instrumented volume of the detector is one cubic kilometer, the actual size of the detector can be larger or smaller, depending on the analyzed particle type and interaction. On the one hand, electron neutrinos and neutral current interactions might require the definition of a veto region. Often the outer string of DOM layers is used for such veto regions, which of course, lowers the volume available for the detection of particle interactions. Muons, on the other hand, can traverse large distances in ice and can consequently be produced far outside the instrumented volume. While this increases the volume available for particle interactions, the lack of knowledge on the interaction vertex at which the muon has been produced is a significant challenge for the reconstruction of neutrino energy spectra (see Section 10.6). Furthermore, the long-range of muons allows atmospheric muons produced in cosmic-ray interactions in the atmosphere to enter the detector in large numbers. Although they are interesting

in themselves, these atmospheric muons are the largest background component in basically all neutrino analyses.

Based on the event signature, atmospheric muons cannot be distinguished from neutrino-induced muons, but the simplest form of background rejection can be achieved via geometrical arguments: as the Earth is opaque for muons, upward-going neutrinos have to originate from neutrino-interactions. Discarding all downward-going muons is thus a promising background rejection strategy.

This strategy comes with a caveat, however: a small fraction of downward going muons will be falsely reconstructed as upward going. Due to the overwhelmingly large number of atmospheric muons relative to atmospheric muons, this *small fraction* still leads to a signal-to-background ratio of approximately 10^{-3} . This remaining background is significantly harder to discard but can be efficiently rejected by the use of machine learning-based analysis techniques. These approaches and, of course, the lessons learned from them, are the subject of this book.

A physics analysis is not complete once the background has been sufficiently rejected. In order to gain physics insight from the data sample, it needs to be analyzed, and physics parameters need to be extracted. A particularly challenging type of analysis in astroparticle physics is the reconstruction of energy spectra. The challenges arise from different sources. First, the underlying processes of particle production are governed by stochastical processes, which are mathematically covered by the Fredholm integral equation of the first kind. This, in turn, means that the sought-after spectrum can only be successfully recovered from distributions of measured observables via the use of deconvolution techniques. Further challenges arise from a secondary amount of smearing introduced by the detector itself. For neutrino telescopes, this additional smearing is mainly introduced by the fact that muons can be produced far outside the detector. While awaiting their detection and traveling towards the detector, these muons consequently lose a certain part of their energy. The energy of the incoming muon (neutrino induced or not) is thus somewhat smaller than the energy of the muon at its production vertex. Electronic noise and uncertainties in the description of impurities in the ice only add to this. It is then the task of the deconvolution algorithm to recover the neutrino energy spectrum from the inaccurately measured distribution of neutrino-induced muons. It becomes quite clear that it is a challenging task that requires a certain amount of algorithmic development. We have thus dedicated an entire chapter to deconvolution for an in-depth coverage of this topic (see Chapter 10).

The quality of spectral reconstruction does improve with the quality of the underlying energy reconstruction, but neutrino telescopes also suffer from their relatively poor angular resolution. IceCube, for example, has an angular resolution of $\approx 0.7^\circ$ for tracks and of $\approx 15^\circ$ for cascades. For comparison, the size of the Sun and the Moon in the sky is on of the order of 1°. A good angular resolution is, however, a prerequisite for the detection of astrophysical neutrino sources. Over the past decade, deep neural networks have been extremely successful in various task areas, e.g., image reconstruction.

Within this book, we also show how neural networks can be applied to reconstruction tasks in neutrino astronomy (see Section 9.2).

Although spread out over several thematic chapters, this book will guide the reader through an entire analysis in neutrino astronomy, ranging from data acquisition (Section 4.2.3), feature selection and track reconstruction (Section 7.2) to background rejection (Section 8.3.1) and finally to the deconvolution of neutrino energy spectra (Section 10.6).

2.2.1.2 Gamma-Ray Astronomy

Lena Linhoff Alicia Fattorini

Just as neutrino astronomy, ground-based gamma astronomy exploits the Cherenkov effect to visualize particles that are not directly accessible. In this case, the Earth's atmosphere is used as a detector medium to observe gamma rays in an energy range from roughly 50 MeV to 30 TeV originating from distant galaxies or supernovae. By measuring and analyzing these particles, we gain knowledge about the gamma-ray sources in the universe, their composition, and the mechanisms that drive their behavior.

If a high-energetic particle, no matter if it is a gamma ray or a charged particle, hits Earth's atmosphere, it produces a cascade of charged particles. These so-called secondary particles inherit a fraction of the primary particle's energy and propagate through the air at high velocities, which might be faster than the speed of light in that medium. The particle cascade emits Cherenkov radiation, which is visible for a few nanoseconds as a large blue to the ultraviolet light cone. From the size, shape, and orientation of this Cherenkov cone, one can derive information about the energy, type, and origin of the primary particle.

Since Cherenkov light is extremely faint and the cone is visible only for a few nanoseconds, a big light collector and camera are needed that are capable of resolving these very short timescales. These requirements are technically realized as Imaging Air Cherenkov Telescopes (IACT). IACTs consist of large spherical mirrors with a diameter of several meters that reflect the Cherenkov light into a camera equipped with pixels that are capable of detecting detect single photons. In very high energy gamma-ray astronomy, the camera pixels typically consist of several hundred photomultiplier tubes (PMT) or silicon photomultipliers (SiPM).

When the camera is triggered by incoming light, a time series of roughly 100 nanoseconds is recorded for every pixel. Based on these time series, the number of photons hitting the pixel and their arrival time are calculated. Once these values are derived, the pixels containing the actual Cherenkov shower are selected from the whole camera image based on their photon charge and arrival time. The selected pixel groups are then parameterized, taking into account their shape, position in the camera, and

light distribution. Once the data is reduced this way, one ends up with a set of parameters belonging to a single event. In modern telescope setups, two or more Cherenkov telescopes are used to observe the same shower from slightly different positions at the same time. This way, the parameter sets of all telescopes are combined, and the position and energy reconstruction can be improved using the information of all observing telescopes. The resulting data set is then used to estimate the primary particle's type, energy, and origin via the data analysis techniques further explained in the following chapters. As soon as the energy and origin are reconstructed, the source's spectral energy distribution and flux variations as a function of time can be computed and studied further.

As already described for neutrino astronomy, gamma-ray astronomers also have to deal with a large background that has to be separated from the actual signal in one of the first steps. With a factor of roughly 10^5 , the background is, in this case, dominated by hadronic particles that induce similar showers as gamma rays. In contrast to gamma ray-induced showers, these showers cannot be traced back to a specific source because charged particles are deflected by magnetic fields on their way through the universe. Therefore they do not carry any source-specific information and have to be separated from the gamma-ray events.

An IACT's observation capacity is limited mostly by sunlight and moonlight and its location on Earth, which restricts the sources that can be observed. Since the Cherenkov showers are very dim and the camera electronics are extremely sensitive, ground-based gamma-ray observations can take place only during nights with no or moderate moonlight and far away from man-made light sources in urban areas. Furthermore, the sky must be transparent for the Cherenkov light, which means that bad weather conditions and clouds heavily affect the observation quality. Therefore IACTs are mostly built at remote places, several hundred to thousands of meters above sea level, to ensure stable observation conditions.

Among other IACTs, the Major Atmospheric Gamma-Ray Imaging Cherenkov Telescopes (MAGIC [47, 48]) are the world's largest operating stereo system. MAGIC is located at the height of 2200 m at the Roque de los Muchachos, the main volcano of the Canary Island, La Palma, Spain. Each telescope has a mirror with a diameter of 17 m, focussing the light into the camera with 1039 PMTs. The telescopes are sensitive to gamma rays with energies between 30 GeV and 100 TeV, depending on observation and trigger settings. The construction of the first telescope was completed in 2004, and the second telescope started operations in 2009. With a series of upgrades in 2011 and 2012, MAGIC got a stereo trigger and readout system to perform measurements in stereo mode.

MAGIC has provided many scientific insights over the years. With the detection of very-high-energy gamma rays from the known blazar, TXS 0506+056 in 2017 [55], a breakthrough was made in the astrophysics community regarding the question of the origin of high-energy cosmic rays. The observed gamma rays were temporally and spatially correlated with a neutrino event reported by IceCube, which confirmed blazars

to be the most promising candidates for neutrino sources. With its lightweight structure based on carbon-fiber tubes, MAGIC is able to reposition with a speed of 7 °/s. After a gamma-ray burst (GRB) was detected with the Swift-BAT satellite in 2019, an alert was sent to the Gamma-ray Coordinates Network (GCN), and MAGIC managed to start observations only 50 seconds after the burst. With this effort, a gamma-ray burst was detected with an IACT for the first time [365, 383].

Next to MAGIC is a second telescope, the First G-APD Cherenkov Telescope (FACT) [53], which was originally designed for employing and testing novel camera technology. It is the first IACT with a camera made of SiPMs (1440 pixels) instead of PMTs. The FACT mirror has a diameter of 3.5 m. The telescope is sensitive to gamma rays with energies from several hundred GeV up to about 10 TeV.



Fig. 2.4: The LST-1 (back) and the FACT (front) at the Roque de los Muchachos Observatory in La Palma, Spain. Photo: Maximilian Linhoff/TU Dortmund University, 2021.

Meanwhile, the new generation of IACTs is under construction. The Cherenkov Telescope Array (CTA) [120] will consist of more than 100 telescopes in La Palma, Spain, and Paranal, Chile, providing a view of the northern and southern skies. Three types of telescopes are planned: Large-, Medium-, and Small-Sized Telescopes, called LSTs, MSTs, and SSTs. Each type has a specific size of the reflector surface and covers a certain energy range, resulting in a wide total energy range from 20 GeV to 300 TeV for the whole telescope array. CTA will be ten times more sensitive than the current generation of IACTs and will have a higher energy resolution. The construction of the first LST at La Palma was completed in 2018, and after the commissioning phase, three further

LSTs will be built at the site. With unprecedented sensitivity from IACT systems, CTA will open a new window on the universe and enable the discovery of new gamma-ray sources.

2.3 Particle Physics

Bernhard Spaan Holger Stevens

The discovery of nuclear fission in 1939 is one of the primary reasons for establishing particle physics. Nowadays, the focus of interest is not on the atomic level but on subatomic elementary particles. These elementary particles are influenced by multiple forces. In the 1970's, a theory was developed that describes the particles and the corresponding forces, known as the standard model of particle physics. With the model, predictions of various physics processes are possible. The most straightforward prediction is the ratio of different decay modes from a so-called mother particle. To test such predictions, such decays must be observed. As the particles of interest are not stable and decay very fast, they needed to be produced in a detector. The particles are produced by accelerators, which collide high energetic particles. From the free energy in the collision, new particles can be formed. This transformation possibility is commonly known as Einstein's equation $E = mc^2$. It is important to note that the produced particles' type, energy, and flight direction are unknown a priori. Therefore one of the main challenges of particle physics detectors is to reconstruct and identify particles. Because they decay fast, this is done indirectly via the reconstruction and combination of their daughter particles. An essential tool is Monte Carlo simulations. They are used before and during the construction of a detector to simulate the expected performance. However, the simulation is also used for cross-checks and error estimations to analyze the actual data.

2.3.1 Experiments

The LHCb experiment at the Large Hadron Collider (LHC) at CERN has been designed to probe the standard model with high precision measurements. The main focus of the experiment is the analysis of particles consisting of at least one heavy quark, the b-quark or its antiparticle, the \bar{b} -quark—sometimes also called the beauty- or bottom quark. The so-called b-hadrons (B-mesons or b-Baryons) are relatively short-lived with a lifetime of about 1.5 ps, thus decaying after traveling on average approximately 1 cm to a few other particles that are long-lived and thus can be detected by the experiment. At the Large Hadron Collider, bunches of protons collide with other bunches of protons

at center-of-mass energies of up to 14 TeV. The collision of heavy ions with heavy ions or heavy ions with protons is also possible. LHCb can take data in all running scenarios. However, the experiment primarily collects proton data. In these collisions, pairs of b-quarks, namely a b and \bar{b} (the anti-b-quark), are copiously produced. However, processes involving the production of lighter quarks or gluons are much more frequent by approximately a factor of 100. In addition, many other particles are produced in a single collision of 2 protons. For example, in a collision of 2 protons where a \bar{b} -pair is produced, only a few percent of all particles visible in the detector stem from the decay of the B-hadrons. b-hadrons have typically several hundred different decay modes where those of interest for the data analyses of LHCb occur only with a fraction of 10^{-3} or less, sometimes as low a $\bar{}$ or even less than that.

Processes of particular interest involve neutral *B*-mesons ($B_s^0: \bar{b}s, B_d^0:: \bar{b}d$) decaying to final states that are sensitive to violation of the symmetry between particles and antiparticles. The analyses of these decays bear the potential to shed some more light on the origin of the *CP*-violation and thus on the mystery of the apparent asymmetry between matter and antimatter in the universe, which the standard model of particle physics cannot explain. The need for precision measurements of these types of decays is the driving factor in the design of the LHCb-experiment. Due to a very subtle mechanism, neutral *B*-mesons can oscillate between particle and antiparticle states during the short time between production and decay ($B\bar{B}$ -oscillations). Since there are certain types of B-meson decays with common final states (CP-eigenstates) for B^0 and anti- B^0 -mesons (\bar{B}^0) , the interference between $(B\bar{B}$ -oscillations and decays into such CP-eigenstate give rise to measurable *CP*-violation effects. The measurements of the magnitude of these CP-asymmetries are then used to probe the standard model of particle physics with precision. The measurement principle is to determine differences between decay rates of B- and \bar{B} -mesons at the time of production t=0 as a function of time until they decay. This measurable asymmetry A_{CP} can be written as follows:

$$A_{CP} = \frac{\Gamma(B^0(\to f_{CP}) - \Gamma(\bar{B}^0(\to f_{CP})) - \Gamma(\bar{B}^0(\to f_{CP}))}{\Gamma(B^0(\to f_{CP}) + \Gamma(\bar{B}^0(\to f_{CP}))},$$
(2.1)

where f_{CP} denotes a CP-eigenstate such as $J/\psi K_S^0$ or D^+D^- . Obviously, it is impossible to tell from the decay final state whether the initially produced meson has been a B- or a \bar{B} meson. Likewise, it is impossible to know whether the decaying meson was a B- or a \bar{B} meson at the time of decay. However, it is essential to determine the "flavor" of the initially produced meson, i.e. B or \bar{B} . As pointed out, the design of the experiments reflects the need to perform these precision measurements. Compared with other large particle physics detectors at the LHC, such as ATLAS or CMS, LHCb has a different shape, as can be seen in Figure 2.5, where cross-sections of CMS and LHCb are shown. CMS is a so-called 4π -Detector, with a maximum coverage symmetrically around the interaction point where the protons collide. By contrast, the interaction point at LHCb is not the center of the detector but almost at one side. The detector topology resembles a forward spectrometer typically used in fixed-target experiments. It thus detects only particles

emitted from the interaction point within an angle between ≈ 15 and ≈ 300 mrad around the beam axis. Although only a tiny fraction of particles produced in a collision can be detected, it turns out that about $\frac{1}{4}$ of all $b\bar{b}$ -quark pairs, and thus their decay products are directed into this region. This phenomenon is caused by the fact that protons are very complex objects, consisting of so-called partons, which consist of 3 valence quarks and a vast number of quark-antiquark pairs as well as gluons. When

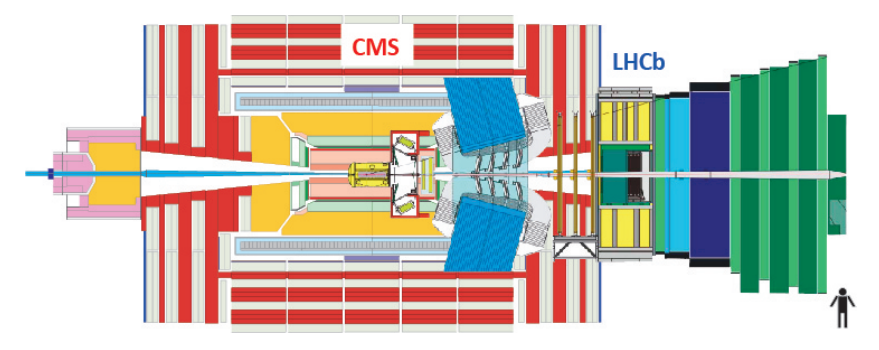


Fig. 2.5: Cross-section of the detectors: CMS (left) and LHCb (right). [244]

two protons collide, the primary interaction at the LHC is typically the interaction of 2 gluons, which may produce a $b\bar{b}$ -quark pair, whereas the remainder of the proton is initially not involved in this process. The momentum of a proton is the sum of the momenta of all partons within the proton. Thus, the partons participating in the primary interaction may carry very different momenta, resulting in a boost of the $b\bar{b}$ -quark pair along the beam axis. Another feature of the strong interactions is that free quarks cannot be observed. It turns out that the binding potential between a quark and an antiquark as a function of the distance between the quarks r can be described as

$$V_{q\bar{q}}(r) \propto -\frac{\alpha}{r} + \kappa r,$$
 (2.2)

where α is the (running) coupling constant of the strong interaction and $\kappa \approx 1 \, \text{GeV/fm}$. Therefore, an energy of $\approx 1 \, \text{GeV}$ is needed to separate two quarks by just $10^{-15} \, \text{m}$. Now consider a $b\bar{b}$ being created with high momenta in opposite directions in the rest frame of both colliding partons. An enormous field-energy will be created between the quarks separating from each other. According to Einstein's famous formula $E = mc^2$, it turns out that it is energetically preferred to create numerous $q\bar{q}$ -pairs out of the field energy, which subsequently find partners to form hadrons such as mesons ($q\bar{q}$ -pairs) and baryons (3 quarks) and antibaryons (3 antiquarks). These newly produced particles are then visible in the detector. This simplified picture should be used to understand what events at the LHC look like. Thus, several hundred particles can be produced in a high-energy proton-proton collision at the LHC within a range of mostly a few femtometer, thus appearing to stem from a single point, known as the primary vertex.

This brings us back to the $b\bar{b}$ -pairs being produced with momenta, which points to the acceptance of the LHCb detector. They will form B-hadrons accompanied by numerous other particles. The lifetime of about $1.5 \cdot 10^{-12} \mathrm{s}$ makes these particles unique. Many other particles will decay almost immediately. Thus they will decay within the range mentioned above of few femtometer. B-hadrons will travel on average ≈ 1 cm before they decay. Only very few charged particles species have lifetimes that allow them to travel through the entire detector: electrons (e^\pm) , muons (μ^\pm) , pions (π^\pm) , kaons (K^\pm) , and protons (p,\bar{p}) , and very light nuclei such as deuterons, which are produced only very rarely. As the decay of B-mesons such as B_d^0 or $B\bar{0}_s^0$ will follow an exponential distribution, the average time between production and decay is thus the lifetime. The actual decay time t can be determined by their flight distance ℓ :

$$\ell = \beta \gamma t, \tag{2.3}$$

where β is the velocity of the *B*-meson *v* divided by the speed of light *c*, and the Lorentz factor *y* is:

$$\gamma = \frac{1}{\sqrt{1 - \beta^2}}.\tag{2.4}$$

As B-mesons ultimately decay into long-lived particles, we can use the measured trajectories of the charged long-lived particles from *B*-meson decays to infer their location of decay known as the secondary vertex. Likewise, the primary vertex can be located similarly. Thus, we have derived a crucial design criterion for the LHCb detector, namely to have the ability to reconstruct primary and secondary vertices with precision. The next design criterion can be easily derived: B-mesons have to be identified, and their momenta have to be measured with precision to derive the decay time from their flight distance ℓ . The LHCb detector is shown in Figure 2.6. Several tracking detectors measure the trajectories of charged particles. At the interaction point, one can find the Vertex Locator (VELO), which is capable of measuring track hits very close to the beamline. The innermost sensors have a radial distance from the beam of just 5 millimeters, which is perilously close compared with other detectors. Using the vertex locator, the track parameters can be measured with high precision, enabling us to extrapolate them towards the beam to find primary and secondary decay vertices. As seen from the interaction point, there is one tracking detector (TT, tracker turicensis) just in front of the magnet, and another tacker just behind the magnet, consisting of the Inner Tracker (IT and the outer Tracker (OT). With the current upgrade of the experiments, all three trackers will be replaced by a new tracking detector. The IT/OT tracker will be replaced by the ScFi-Tracker (Scintillating Fibre), whereas Upstream Tracker (UT) has a very similar sensor technology to the TT. The Upgraded VELO will now contain a pixilated sensor, increasing the number of channels significantly. With tracking detectors in front of and after the magnet, the bending of the charged tracks in the magnetic field can be measured, which enables the determination of their momenta. However, several ingredients are still missing as we need to know which type of particles have been measured. This is highly relevant for the measurements on *CP*-violation or rare decays

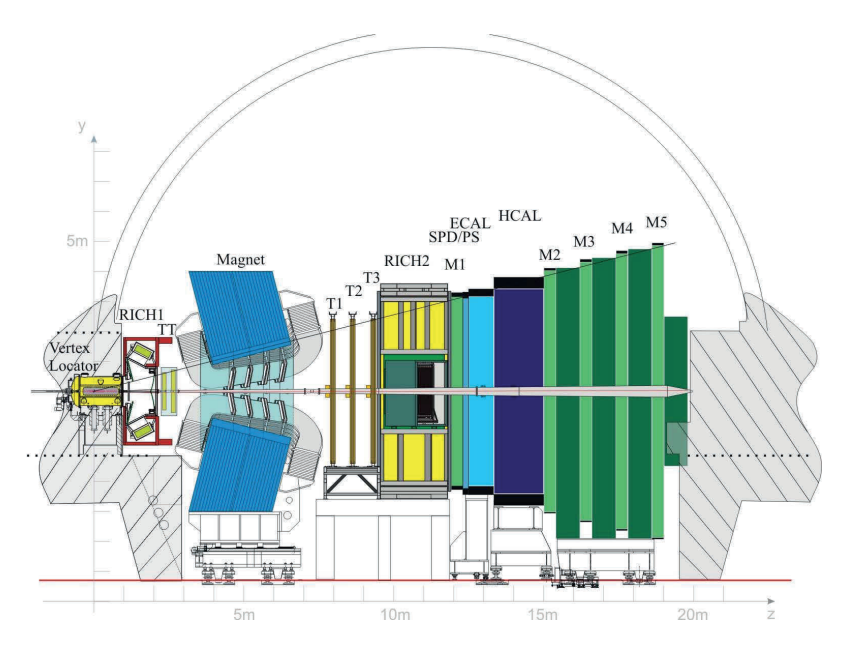


Fig. 2.6: The LHCb detector. [51]

of *B*-mesons. Therefore, the next design criterion is to have *the capability of identifying the different particles in a given event.*

Several sub-detectors are devoted to this task. The sub-detector furthest away from the interaction point is known as the Muon system, a dedicated muon identification system. This system identifies muons by particles traversing the detector because all other particle species will be absorbed by the calorimeters and the absorbers of the muon system with the highest probability. Typically, all detectors at particle colliders will have a muon system, as the presence of muon is an excellent indication of an exciting physics process in the event. The aforementioned calorimeters consist of an electromagnetic calorimeter followed by the hadron calorimeter. Contrary to all other charged particles with high momentum, the electron will be stopped in the calorimeter and thus deposit its total energy. The measurement of the deposited energy, together with the momentum, provides information about the presence of an electron. The other large detectors are equipped with calorimeters and muon systems.

Identifying pions, kaons, and protons is a bit more complex, as, unlike electrons and muons, they do not have specific properties that allow their identification. However, they have different masses, which results in particles with the same momentum having different velocities. Thus, a measurement of the velocity can be used to infer the mass of a particle when the momentum is known. Due to the relativistic nature of particles with high momenta, the velocity of the particles with different masses is very similar, making a direct measurement of the velocity difficult. However, using Ring-Imaging Cherenkov detectors, information on the velocity of high momentum particles can be

It might appear that the purpose of the calorimeters is mainly to identify electrons and absorb other particles. The electromagnetic calorimeter is responsible for measuring the energy of lighter particles, such as electrons and photons, while the hadron calorimeter samples the energy of hadrons, i.e., protons, neutrons, and other particles containing quarks. In principle, the detector components are now available to perform the measurements. However, the data from the sub-detectors must be transformed into physical quantities used in the analysis. For example, individual hits in an event need to be associated with a track, for which the momentum must be determined. This will be discussed later.

The measurement of A_{CP} shall now be described to illustrate the interplay of the various sub-detector components. The decay channel $B^0 \to J/\psi K_S^0$ is known as a golden mode, which has a large CP-asymmetry and very little theoretical uncertainties in the interpretation of the measurement. The J/ψ is a short-lived meson, which is reconstructed in the decay mode $J/\psi \to \mu^+\mu^-$. Thus, the excellent muon identification capabilities ensure the proper selection of the signal. The K_S^0 -meson is reconstructed in the decay mode $K_S^0 \to \pi^+\pi^-$. The electrically K_S^0 has a lifetime of $\approx 10^{-10} \mathrm{s}$ which results in much larger decay flight distances of up to $O(1\,\mathrm{m})$ when compared with that of the B^0 -meson. Therefore, the precision of determination of the secondary decay vertex of the B^0 -meson relies mainly on the proper reconstruction of the J/ψ decay vertex. From the measured momenta $\vec{p}_{\mu\mu} = p_{\mu^+} + p_{\mu^-}$ and energies $E_{\mu\mu} = E_{\mu^+} + E_{\mu^-}$ of the muons, it is straight forward to determine the invariant mass $m_{\mu\mu}$ of the system:

$$m_{\mu\mu}c^2 = \sqrt{E_{\mu\mu}^2 - p_{\mu\mu}^2 c^2}$$
.

The reconstructed invariant dimuon mass spectrum has a shape that resembles a Gaussian distribution on top of some background. A typical invariant mass spectrum indicates signal (J/ψ) and background. Figure 2.7 depicts the general shape of the spectrum and a certain background level. The presence of background is due to several sources. For example, combinatorial background arises if two muon candidates are combined where one or two of the muons candidate do not stem from the J/ψ decay. Their respective invariant math will cover a wide mass range, whereas in the signal case, the invariant mass shape follows mainly the mass resolution.

In addition, there is the possibility that a muon candidate is identified as a muon. This might happen with a relatively low probability should, say, a hadron not be absorbed. Although the individual survival probability is very low, the number of hadrons is significantly larger than the number of true muons in the events. The data analysis has a handle to change the background level. For example, the information on the

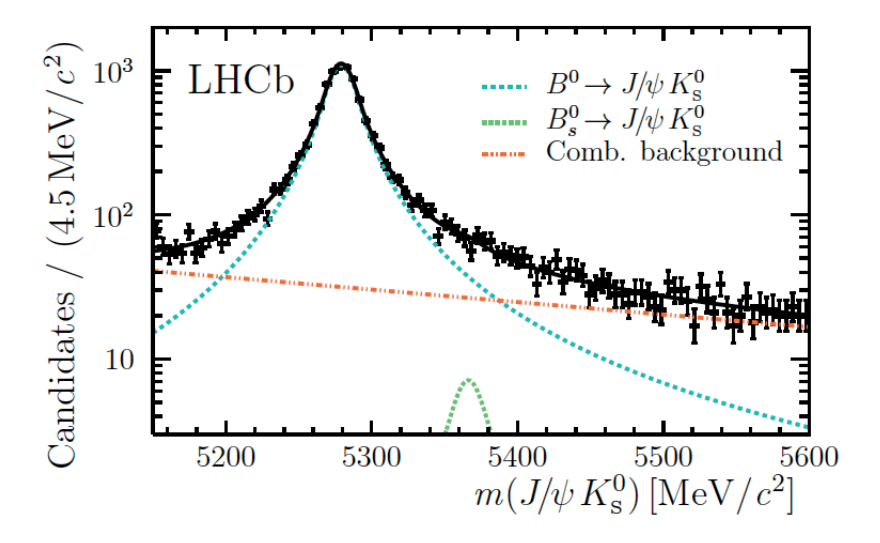


Fig. 2.7: Illustration of a typical invariant $\mu^+\mu^-$ mass distribution, depicting signal and background.

quality of the secondary vertex reconstruction can be used to reduce the probability of combining particles that do not originate from the same (secondary) vertex. Similarly, the K_S^0 -mesons will be reconstructed from two oppositely charged pion candidates. There are some possible backgrounds, such as decays from other similarly long-lived particles decaying, for example, to a proton and a pion. Again, the misidentification of particles gives rise to background levels. As pointed out, particle identification using various sub-detectors comes with a certain misidentification probability. In order to minimize the misidentification probability, the information provided by all sub-detectors is combined to form a single variable called ProbNN. The combination turns out to be complex and is based on a neural network approach that gives variables their name.

In principle, reconstructing B^0 -mesons candidates from J/ψ - and K^0_S -candidates follows the same procedure by determining the energy and momentum of the B^0 candidate by adding energies and momenta of the J/ψ - and K^0_S -candidates. However, for basically all analyses, it is of utmost importance to minimize the effects of backgrounds on the measurement of, e.g., CP-asymmetries. Accepting only J/ψ - and K^0_S -candidates with masses in the range defined by the resolution function is standard practice. Many other criteria can also be used to optimize the selection further. In most analyses, machine learning methods are used to achieve an optimal selection. Boosted decision trees or neural nets are typically used.

The selection of the signal channel to measure *CP*-asymmetries is just the first step. As pointed out, it is necessary to determine momentum and flight distance to derive the decay time of the particle. The momentum is known after the selection. To

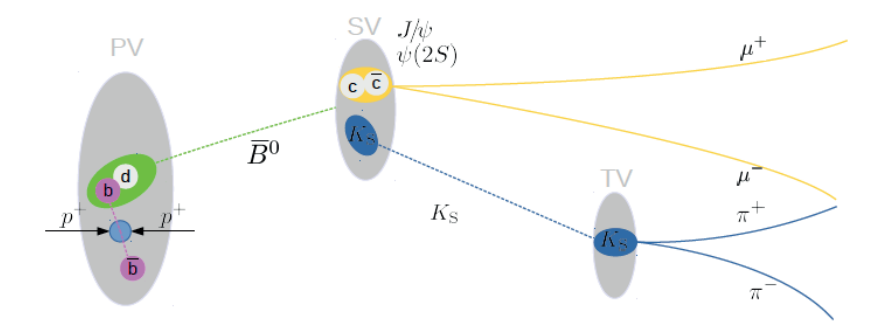


Fig. 2.8: Illustration of a typical B-decay topology. Charged tracks emerging from the primary vertex and other vertices are depicted as solid straight lines. The tracks are extrapolated using the track parameters determined by the tracking systems. The B^0 -meson (dashed-dotted red line) travels on average ≈ 1 cm before it decays—in this case: $B^0 \to J/\psi K_S^0$. The J/ψ would decay almost instantaneously, where for the analysis, the decay into two leptons is relevant $(\mu^+\mu^-, e^+e^-)$. The K_S^0 -meson (dashed-dotted green line) has a considerably longer lifetime than B-mesons.

determine the flight distance, the charged tracks associated with the reconstructed B-candidate are used to reconstruct the secondary vertex of the B-meson. Therefore, the measured track parameters of the track are used to extrapolate the trajectory of the track towards the beamline. Due to the long lifetime of the K_S^0 -mesons, the extrapolation of the track parameters of the pions will have considerably larger errors at the location of the B decay vertex. Thus, the precision in the measured vertex positions arises mainly from the muon track parameters. The location of the primary vertex can be readily determined from the numerous other tracks in the event. A sketch of the decay topology is shown in Figure 2.8.

The next ingredient of analysis is called tagging, the determination of the "flavor" of the B^0 -meson under consideration at the production time. The determination of whether it was a B^0 or a $\bar{B^0}$ at t=0 relies on the fact that B-quarks are produced in pairs. Since only a fraction of the produced b-quarks will end up in neutral B-mesons, information on the other B-hadron produced in the same reaction will provide an answer. There is more useable information in the event, say, from mesons produced close to the neutral B-meson under consideration. In order to retrieve the desired information, excellent particle identification capabilities are necessary—another strong constraint in the design criteria for the LHCb experiment. Despite the excellent detector, the probability of having a proper tag in a given event is very small.

What is known as tagging power ϵ_{eff} quantifies the effective statistical reduction of the data sample due to imperfections in the tagging. Thus, the statistical uncertainty σ on a time-dependent asymmetry measured on a sample of size N depends on ϵ_{eff} as

 $\sigma \propto 1/\sqrt{N}$. The tagging power depends on the channel in which the *CP*-asymmetry is measured. Despite all efforts, its value is typically well below 10 %. Therefore, LHCb invests a continued large effort to improve the tagging power. A doubling of the tagging power corresponds to doubling the data sample with no further improvement, which amounts to several years of data taking. In order to obtain the highest possible tagging power, new tagging methods are being developed, based on deep neural networks.

Obviously, it is necessary to determine the efficiency of the detection and extraction of physical observables such as CP-asymmetries. In addition, the influence of backgrounds present in the data set needs to be known with high precision. For this type of task, extensive Monte Carlo simulations are typically used.